Unified Vibration Suppression and Compliance Control for Flexible Joint Robot

CUI Shipeng, SUN Yongjun, LIU Yiwei, LIU Hong*

State Key Laboratory of Robotics and System, Harbin Institute of Technology, Harbin 150001, P. R. China

(Received 6 May 2020; revised 30 June 2020; accepted 8 September 2020)

Abstract: An adaptive control scheme is presented, which can simultaneously realize vibration suppression and compliance control for flexible joint robot (FJR). The proposed control scheme provides a unified formulation for both vibration suppression mode, where FJR tracks the desired position with little vibration, and compliance mode, in which FJR presents passive. Instead of designing multiple controllers and switching between them, both modes are integrated into a single controller, and the transition between two modes is smooth and stable. The stability of the closed-loop system is theoretically proven via the Lyapunov method, with the considering the dynamics uncertainties in both link side and motor side. Simulation results are presented to illustrate good performances of the proposed control scheme.

Key words: adaptive control scheme; vibration suppression; compliance; flexible joint robot (FJR); stability

CLC number: TP242 **Document code:** A **Article ID:** 1005-1120(2021)03-0361-12

0 Introduction

Recently, interest in flexible joint robot (FJR) which possesses inherent compliance has been greatly increased[1-4]. Unlike rigid robots, FJR's joint contains an elastic element, which introduces a lower mechanical output impedance, passive mechanical energy storage, and increases peak power output. Moreover, the inherent compliance brought by the elastic element can filter impact, protect drivetrains, and provide additional time for controller to regulate the impedance of FJR. Due to the above characteristics, FJRs are widely used in the field of physical interactions with the surroundings or humans, such as rehabilitation robots, exoskeleton or wearable robots and assembly robots. In those applications involving physical interactions, safety of FJRs and the surroundings or humans is always the most critical concern when controlling the position of FJR. Therefore, the purpose of this paper is to design a control scheme to realize the position control of FJR and ensure the safety of FJR and the surroundings or humans.

Elastic element will bring much difficulty to position control of FJR comparing with that of rigid ones. Firstly, due to the existence of elastic element, the dynamics of FJR is decoupled into two parts: Motor side and link side, which are described by a second-order nonlinear equation, thus, the order becomes twice that of the rigid joint. This poses a nontrivial task due to the increase of the model complexity. Secondly, the number of control inputs is strictly less than mechanical degrees of freedom, which illustrates that FJR is a nonlinear, under-actuated and strong coupling system. Moreover, FJR is prone to vibrate, which deteriorates system stability and requires extra power for position control. Several approaches have been proposed to control the position of FJR. Tomei[5] proved that a simple proportional-differential (PD) controller can globally stabilize about a reference position. Kim et al.[6] proposed a robust PD control scheme for FJR based on a disturbance observer (DOB) which was only applied to the motor-side dynamics. Jin et al.[7] de-

*Corresponding author, E-mail address: sunyongjun@hit.edu.cn.

How to cite this article: CUI Shipeng, SUN Yongjun, LIU Yiwei, et al. Unified vibration suppression and compliance control for flexible joint robot[J]. Transactions of Nanjing University of Aeronautics and Astronautics, 2021, 38(3): 361-372.

http://dx.doi.org/10.16356/j.1005-1120.2021.03.001

signed an adaptive tracking controller using a time-delay estimation technique. Mobayen et al.[8-9] proposed sliding mode control techniques for a class of fourth-order system which can describe the position control system of FJR. Besides, a variety of vibration suppression control schemes have been developed for FJR. As an effective method, damping dissipation strategy has been studied in the literature. Well-known implementations of damping dissipation strategy include feedback linearization[10], model-based state-feedback controllers[11], learning control schemes[12], and linear-quadratic regulators[13]. Other effective approaches focusing on the vibration attenuation of FJR through joint motion input include input shaper[14] and singular perturbation control[15]. Besides, resonance ratio control (RRC)[16] and overshoot control[17] can also effectively suppress vibration of FJR.

The aforementioned control methods only focus on the position control problem. For FJR, which is designed to closely interact with the surroundings, the safety between FJR and the surroundings should be also considered. In order to complete position control and meanwhile achieve compliance in control, hybrid position/force control[18] and impedance/admittance control[19] have been proposed for robot. Nevertheless, the hard switching of hybrid position/force control may result in an overall discontinuous control input, which further causes the chattering movement of robot or even compromises the safety of robot and the surroundings. Impedance/admittance controllers have no discontinuity during switching, but the desired impedance has to be adjusted according to the intention of human. In addition, most aforementioned control schemes commonly assume the robot dynamics to be exactly known, and do not take the uncertainty of model parameters into account. Continuous control techniques for the human-robot interaction have been proposed[20-21], but these schemes have no focus on the position control with vibration suppression. As for as we know, there is no research on unified vibration suppression and compliance control scheme.

In this paper, a novel continuous adaptive control scheme which integrates both modes, i.e., vibration suppression mode and compliance mode, into a single controller, is proposed for FJR. The proposed controller is able to automatically transit between both modes, and the transition between two modes is smooth and stable. A stability analysis is performed for the closed-loop system with considering the dynamics uncertainties in both link side and motor side. Simulation results are given to show the validity of the proposed control scheme. The main novelties can be summarized as follows:

(1) A unified control scheme which integrates both modes of vibration suppression and compliance into a single controller is first designed for FJR.

(2) The proposed control scheme is performed well with considering the dynamics uncertainties in both link side and motor side by means of suitable adaptive laws.

(3) The proposed control scheme is rather straightforward and easily implemented in engineering.

1 Problem Description

According to the Spong's assumptions[22], dynamics of FJR with high gear reduction consists of two parts coupled through the elastic element, that is, link-side dynamics

$$\boldsymbol{M}(\boldsymbol{q})\ddot{\boldsymbol{q}}+\boldsymbol{C}(\boldsymbol{q},\dot{\boldsymbol{q}})\dot{\boldsymbol{q}}+\boldsymbol{D}_q\dot{\boldsymbol{q}}+\boldsymbol{g}(\boldsymbol{q})=\boldsymbol{K}(\boldsymbol{\theta}-\boldsymbol{q})+\boldsymbol{\tau}_e \tag{1}$$

and motor-side dynamics

$$\boldsymbol{B}\ddot{\boldsymbol{\theta}}+\boldsymbol{D}_\theta\dot{\boldsymbol{\theta}}+\boldsymbol{K}(\boldsymbol{\theta}-\boldsymbol{q})=\boldsymbol{\tau} \tag{2}$$

where $\boldsymbol{q}\in\mathbb{R}^n$ and $\boldsymbol{\theta}\in\mathbb{R}^n$ are the position vector of link side and motor side, respectively. $\boldsymbol{M}(\boldsymbol{q})\in\mathbb{R}^{n\times n}$ is the inertia matrix of link side, $\boldsymbol{C}(\boldsymbol{q},\dot{\boldsymbol{q}})\dot{\boldsymbol{q}}\in\mathbb{R}^n$ the Coriolis and centripetal torque vector of link side, $\boldsymbol{g}(\boldsymbol{q})\in\mathbb{R}^n$ the gravity vector of link side, $\boldsymbol{K}\in\mathbb{R}^{n\times n}$ the stiffness matrix of FJR, and $\boldsymbol{B}\in\mathbb{R}^{n\times n}$ the inertia matrix of motor side. $\boldsymbol{D}_q\dot{\boldsymbol{q}}\in\mathbb{R}^n$ and $\boldsymbol{D}_\theta\dot{\boldsymbol{\theta}}\in\mathbb{R}^n$ are the viscous friction vectors of link side and motor side, respectively. $\boldsymbol{\tau}_e=\boldsymbol{J}^{\mathrm{T}}(\boldsymbol{q})\boldsymbol{f}_e\in\mathbb{R}^n$ is the vector of external torque, where $\boldsymbol{J}^{\mathrm{T}}(\boldsymbol{q})\in\mathbb{R}^{n\times m}$ is the transpose of Jacobian matrix $\boldsymbol{J}(\boldsymbol{q})$ and $\boldsymbol{f}_e\in\mathbb{R}^m$ the vector of continuous external force. $\boldsymbol{\tau}\in\mathbb{R}^n$ is the vector of input torque exerted on motor side.

Some important properties of the FJR's dy-

namics described by Eq.(1) and Eq.(2) are listed as follows:

(1) Matrices $\boldsymbol{M}(\boldsymbol{q})$ and $\boldsymbol{B}$ are positive definite;

(2) Matrix $\dot{\boldsymbol{M}}(\boldsymbol{q})-2\boldsymbol{C}(\boldsymbol{q},\dot{\boldsymbol{q}})\dot{\boldsymbol{q}}$ is skew-symmetric;

(3) Viscous friction matrices $\boldsymbol{D}_q=\mathrm{diag}(d_{q1},\cdots,d_{qn})$ and $\boldsymbol{D}_\theta=\mathrm{diag}(d_{\theta 1},\cdots,d_{\theta n})$ are diagonal and positive definite, where d_{qi} and $d_{\theta i}$ are physical parameters;

(4) Gravity vector $\boldsymbol{g}(\boldsymbol{q})$ is linear in a set of physical parameters $\boldsymbol{p}_q=[p_{q1},\cdots,p_{qn_q}]^{\mathrm{T}}\in\mathbb{R}^{n_q}$ as follows

$$\boldsymbol{g}(\boldsymbol{q})=\boldsymbol{Y}_q(\boldsymbol{q})\boldsymbol{p}_q \tag{3}$$

where $\boldsymbol{Y}_q(\boldsymbol{q})\in\mathbb{R}^{n\times n_q}$ is a known dynamic regression matrix;

(5) First two terms of motor-side dynamics are linear in a set of physical parameters $\boldsymbol{p}_\theta=[\boldsymbol{p}_{\theta b}^{\mathrm{T}},\boldsymbol{p}_{\theta d}^{\mathrm{T}}]^{\mathrm{T}}\in\mathbb{R}^{2n}$ as follows

$$\boldsymbol{B}\ddot{\boldsymbol{\theta}}+\boldsymbol{D}_\theta\dot{\boldsymbol{\theta}}=\boldsymbol{Y}_\theta(\dot{\boldsymbol{\theta}},\ddot{\boldsymbol{\theta}})\boldsymbol{p}_\theta=[\boldsymbol{Y}_{\theta b}(\ddot{\boldsymbol{\theta}})\quad\boldsymbol{Y}_{\theta d}(\dot{\boldsymbol{\theta}})]\boldsymbol{p}_\theta \tag{4}$$

where $\boldsymbol{Y}_{\theta b}(\ddot{\boldsymbol{\theta}})=\mathrm{diag}(\ddot{\theta}_1,\cdots,\ddot{\theta}_n)\in\mathbb{R}^{n\times n}$ and $\boldsymbol{Y}_{\theta d}(\dot{\boldsymbol{\theta}})=\mathrm{diag}(\dot{\theta}_1,\cdots,\dot{\theta}_n)\in\mathbb{R}^{n\times n}$ are known and diagonal regression matrices.

In this paper, the dynamic uncertainties in both link side and motor side are taken into consideration, in the sense that the dynamic models $\boldsymbol{M}(\boldsymbol{q})$, $\boldsymbol{C}(\boldsymbol{q},\dot{\boldsymbol{q}})$, $\boldsymbol{D}_q$, $\boldsymbol{g}(\boldsymbol{q})$, $\boldsymbol{B}$, and $\boldsymbol{D}_\theta$ are unknown. $\boldsymbol{K}$ is assumed to be well defined, which is obviously reasonable because the actual stiffness of FJR can be achieved by means of loading calibration experiments. Control objective is to design a unified control strategy including vibration suppression mode and compliance control mode, to ensure a stable and smooth transition between both modes under Properties 1—5 and dynamic uncertainties. In addition, when in vibration suppression mode, $\boldsymbol{q}(t)$ can reach the desired position $\boldsymbol{q}_d$ with little vibration as possible, i.e.

$$\lim_{t\to\infty}\boldsymbol{e}_q(t)=\boldsymbol{0} \tag{5}$$

where $\boldsymbol{e}_q=\boldsymbol{q}-\boldsymbol{q}_d$.

2 Controller Design

In this section, an adaptive unified controller is proposed for FJR, which smoothly integrates both modes, i.e., vibration suppression mode and compliance mode, into a single controller.

2.1 Force region function and weight factor

A force region function is proposed to monitor the variation of external force $\boldsymbol{f}_e$ as[20]

$$\beta(\boldsymbol{f}_e)=\|\boldsymbol{f}_e\|^2-R^2 \tag{6}$$

where R is a positive constant that denotes the radius of force region. When $\boldsymbol{f}_e$ is inside the force region, $\beta(\boldsymbol{f}_e)\leqslant 0$, and vice versa.

Based on force region, a weight factor is defined as[23]

$$\omega(\boldsymbol{f}_e)=1-\frac{1}{1+\exp(-\kappa\beta(\boldsymbol{f}_e))} \tag{7}$$

where $\kappa\gg 1$ is a positive constant. An illustration of weight factor $\omega(\boldsymbol{f}_e)$ is shown in Fig.1, where $\boldsymbol{f}_e=[f_{e1},f_{e2}]^{\mathrm{T}}\in\mathbb{R}^2$.

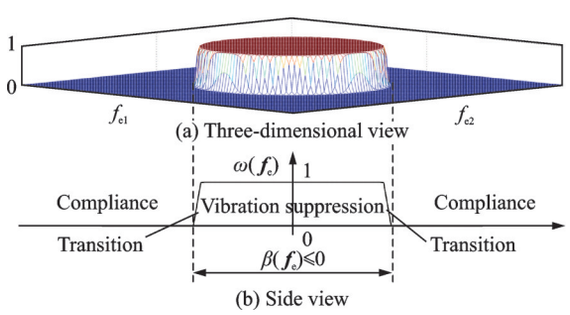

Fig.1 Illustration of $\omega(\boldsymbol{f}_e)$

From Fig.1, when $\boldsymbol{f}_e$ is inside the force region such that $\beta(\boldsymbol{f}_e)\leqslant 0$, $\omega(\boldsymbol{f}_e)=1$. When $\boldsymbol{f}_e$ exceeds the force region such that $\beta(\boldsymbol{f}_e)>0$, $\omega(\boldsymbol{f}_e)=0$. Different values of weight factor will be utilized in vibration suppression mode and compliance mode.

2.2 Desired input for link side

Introducing the position error of motor side $\boldsymbol{e}_\theta=\boldsymbol{\theta}-\boldsymbol{\theta}_d$, then Eq.(1) can be rewritten as

$$\boldsymbol{M}(\boldsymbol{q})\ddot{\boldsymbol{q}}+[\boldsymbol{C}(\boldsymbol{q},\dot{\boldsymbol{q}})+\boldsymbol{D}_q]\dot{\boldsymbol{q}}+\boldsymbol{g}(\boldsymbol{q})+\boldsymbol{K}\boldsymbol{q}=\boldsymbol{K}\boldsymbol{\theta}_d+\boldsymbol{K}\boldsymbol{e}_\theta+\boldsymbol{\tau}_e \tag{8}$$

The desired input $\boldsymbol{\theta}_d$ is considered as a fictitious input for link side, and $\boldsymbol{e}_\theta$ represents an input perturbation to the link-side dynamics. Eq.(8) can be viewed as being controlled by the input $\boldsymbol{K}\boldsymbol{\theta}_d$ with the perturbation of $\boldsymbol{K}\boldsymbol{e}_\theta$.

By using weight factor $\omega(\boldsymbol{f}_e)$, a desired input for link side is presented as follows

$$\boldsymbol{\theta}_d = \boldsymbol{q} - \boldsymbol{K}^{-1}\{\omega(\boldsymbol{f}_e)[\boldsymbol{K}_p \arctan(\boldsymbol{\gamma}\boldsymbol{e}_q) + \boldsymbol{K}_d\dot{\boldsymbol{q}}] - \boldsymbol{Y}_q(\boldsymbol{q})\hat{\boldsymbol{p}}_q - \omega(\boldsymbol{f}_e)\boldsymbol{s}\} \tag{9}$$

where $\boldsymbol{K}_p \in \mathbb{R}^n$, $\boldsymbol{K}_d \in \mathbb{R}^n$ and $\boldsymbol{\gamma} \in \mathbb{R}^n$ are positive definite diagonal matrix. $\hat{\boldsymbol{p}}_q$ is the estimate of $\boldsymbol{p}_q$, which is updated by

$$\dot{\hat{\boldsymbol{p}}}_q = -\boldsymbol{\Gamma}_q \boldsymbol{Y}_q^{\mathrm{T}}(\boldsymbol{q})\dot{\boldsymbol{q}} \tag{10}$$

where $\boldsymbol{\Gamma}_q \in \mathbb{R}^{n_q \times n_q}$ is a positive definite matrix. In Eq.(9), $\boldsymbol{s} = [s_1, s_2, \cdots, s_n]^{\mathrm{T}}$ is the vibration suppression term, with each element detailed as

$$s_i = [-\alpha_{1i} + [\alpha_{2i}\mathrm{sign}(e_{qi}) + \alpha_{3i}\mathrm{sign}(\dot{q}_i)]\left|e_{qi}\right|^{1/2}]\dot{q}_i - \rho_i\dot{q}_i\sum_{j=1}^{n}\dot{\theta}_j^2 \tag{11}$$

where α_{1i}, α_{2i}, α_{3i} and ρ_i are positive constants to be designed, $\mathrm{sign}(\cdot)$ is a standard signum function.

Remark 1 In Eq.(9), the saturated nonlinear term of $\boldsymbol{e}_q$ ensures that link side has a larger control input compared with the normal proportional control term when link-side position error $\boldsymbol{e}_q$ is small; Vibration suppression term $\boldsymbol{s}$ is utilized to add dissipativeness to FJR system, which will help to suppress residual vibration.

The desired fictitious input $\boldsymbol{\theta}_d$ integrates vibration suppression mode and compliance mode as follows:

(1) Vibration suppression mode: When the external force $\boldsymbol{f}_e$ is inside the force region where $\beta(\boldsymbol{f}_e) \leqslant 0$, $\omega(\boldsymbol{f}_e) = 1$, the desired input for link side becomes

$$\boldsymbol{\theta}_d = \boldsymbol{q} - \boldsymbol{K}^{-1}[\boldsymbol{K}_p \arctan(\boldsymbol{\gamma}\boldsymbol{e}_q) + \boldsymbol{K}_d\dot{\boldsymbol{q}} - \boldsymbol{Y}_q(\boldsymbol{q})\hat{\boldsymbol{p}}_q - \boldsymbol{s}] \tag{12}$$

where position control term $\boldsymbol{K}_p \arctan(\boldsymbol{\gamma}\boldsymbol{e}_q)$ and velocity control term $\boldsymbol{K}_d\dot{\boldsymbol{q}}$ drive link side to track the desired position $\boldsymbol{q}_d$.

(2) Compliance mode: When external force $\boldsymbol{f}_e$ is outside the force region where $\beta(\boldsymbol{f}_e) > 0$, $\omega(\boldsymbol{f}_e) = 0$, the desired input for link side is simplified as

$$\boldsymbol{\theta}_d = \boldsymbol{q} + \boldsymbol{K}^{-1}\boldsymbol{Y}_q(\boldsymbol{q})\hat{\boldsymbol{p}}_q = \boldsymbol{q} + \boldsymbol{K}^{-1}\hat{\boldsymbol{g}}(\boldsymbol{q}) \tag{13}$$

where $\hat{\boldsymbol{g}}(\boldsymbol{q})$ is the estimate of gravity vector $\boldsymbol{g}(\boldsymbol{q})$. Eq.(13) leads to the link-side dynamics as

$$\boldsymbol{M}(\boldsymbol{q})\ddot{\boldsymbol{q}} + \boldsymbol{C}(\boldsymbol{q},\dot{\boldsymbol{q}})\dot{\boldsymbol{q}} + \boldsymbol{D}_q\dot{\boldsymbol{q}} + \boldsymbol{g}(\boldsymbol{q}) - \hat{\boldsymbol{g}}(\boldsymbol{q}) = \boldsymbol{K}\boldsymbol{e}_\theta + \boldsymbol{\tau}_e \tag{14}$$

The use of the adaptation in Eq.(10) ensures the convergence of the prediction error, thus $\hat{\boldsymbol{g}}(\boldsymbol{q}) \to \boldsymbol{g}(\boldsymbol{q})$. In addition, if the motor-side position $\boldsymbol{\theta}$ tracks the desired input $\boldsymbol{\theta}_d$ such that $\boldsymbol{e}_\theta = \boldsymbol{\theta} - \boldsymbol{\theta}_d \to 0$, we have

$$\boldsymbol{M}(\boldsymbol{q})\ddot{\boldsymbol{q}} + \boldsymbol{C}(\boldsymbol{q},\dot{\boldsymbol{q}})\dot{\boldsymbol{q}} + \boldsymbol{D}_q\dot{\boldsymbol{q}} = \boldsymbol{\tau}_e \tag{15}$$

which is a damping system, in the sense that external force $\boldsymbol{f}_e$ is able to control link side and the link side shows compliance.

2.3 Adaptive observer and control input for motor side

In this section, control input $\boldsymbol{\tau}$ for motor side is developed such that motor-side position $\boldsymbol{\theta}$ tracks the desired input $\boldsymbol{\theta}_d$, i.e., $\boldsymbol{e}_\theta \to 0$.

A sliding vector is introduced for motor side as

$$\boldsymbol{e}_{s\theta} = \dot{\boldsymbol{\theta}} - \dot{\boldsymbol{\theta}}_r = \dot{\boldsymbol{e}}_\theta + \lambda_\theta\boldsymbol{e}_\theta \tag{16}$$

where λ_θ is a positive constant, and $\dot{\boldsymbol{\theta}}_r$ is a reference vector which is defined as

$$\dot{\boldsymbol{\theta}}_r = \dot{\boldsymbol{\theta}}_d - \lambda_\theta\boldsymbol{e}_\theta \tag{17}$$

Control input for motor side is now proposed as

$$\boldsymbol{\tau} = \boldsymbol{K}(\boldsymbol{\theta} - \boldsymbol{q}) - \boldsymbol{K}_\theta\boldsymbol{e}_{s\theta} + \boldsymbol{Y}_\theta(\dot{\boldsymbol{\theta}}_r, \ddot{\boldsymbol{\theta}}_r)\hat{\boldsymbol{p}}_\theta \tag{18}$$

where $\boldsymbol{K}_\theta$ is a positive definite matrix and $\hat{\boldsymbol{p}}_\theta$ the estimate of motor-side uncertain dynamic parameters vector $\boldsymbol{p}_\theta$, which is updated by

$$\dot{\hat{\boldsymbol{p}}}_\theta = -\boldsymbol{\Gamma}_\theta\boldsymbol{Y}_\theta^{\mathrm{T}}(\dot{\boldsymbol{\theta}}_r, \ddot{\boldsymbol{\theta}}_r)\boldsymbol{e}_{s\theta} \tag{19}$$

where $\boldsymbol{\Gamma}_\theta \in \mathbb{R}^{2n \times 2n}$ is a positive definite matrix.

Note that the control input Eq.(18) for FJR is dependent on the derivatives of desired input $\dot{\boldsymbol{\theta}}_d$ and $\ddot{\boldsymbol{\theta}}_d$, hence, the acceleration information $\ddot{\boldsymbol{q}}$ and its derivatives are required. We consider the uncertain dynamics problem and propose an adaptive observer to estimate the desired input $\boldsymbol{\theta}_d$, thus eliminating the requirement for acceleration and its derivatives. The adaptive observer is as follow

$$\begin{cases} \dot{\hat{\boldsymbol{\theta}}}_d = \boldsymbol{\phi} + \lambda_o\boldsymbol{e}_o \\ \dot{\boldsymbol{\phi}} = \hat{\boldsymbol{B}}_o^{-1}[\boldsymbol{\tau} - \boldsymbol{K}(\boldsymbol{\theta} - \boldsymbol{q}) - \hat{\boldsymbol{D}}_{\theta o}\boldsymbol{\phi} + \boldsymbol{K}_e\boldsymbol{e}_o] \end{cases} \tag{20}$$

where $\hat{\boldsymbol{\theta}}_d$ denotes the estimate of $\boldsymbol{\theta}_d$, $\boldsymbol{e}_o = \boldsymbol{\theta}_d - \hat{\boldsymbol{\theta}}_d$ the observation error, $\boldsymbol{\phi}$ an auxiliary variable, λ_o a positive constant, and $\boldsymbol{K}_e$ a positive definite matrix. Matrices $\hat{\boldsymbol{B}}_o$ and $\hat{\boldsymbol{D}}_{\theta o}$ denote the estimate of $\boldsymbol{B}$ and

$\boldsymbol{D}_\theta$, respectively, which are updated through the following two adaptation laws

$$\begin{cases}\dot{\hat{\boldsymbol{p}}}_{\theta bo}=-\boldsymbol{\Gamma}_{\theta bo}\boldsymbol{Y}_{\theta b}(\dot{\boldsymbol{\phi}})\boldsymbol{z}\\ \dot{\hat{\boldsymbol{p}}}_{\theta do}=-\boldsymbol{\Gamma}_{\theta do}\boldsymbol{Y}_{\theta d}(\boldsymbol{\phi})\boldsymbol{z}\end{cases}\tag{21}$$

where $\boldsymbol{z}=\dot{\boldsymbol{\theta}}-\boldsymbol{\phi}$, $\hat{\boldsymbol{p}}_{\theta bo}=[\hat{b}_{o1},\cdots,\hat{b}_{on}]^{\mathrm{T}}\in\mathbb{R}^n$ and $\hat{\boldsymbol{p}}_{\theta do}=[\hat{d}_{\theta o1},\cdots,\hat{d}_{\theta on}]^{\mathrm{T}}\in\mathbb{R}^n$ are estimated vectors formed by diagonal elements of $\boldsymbol{B}$ and $\boldsymbol{D}_\theta$, respectively. $\boldsymbol{\Gamma}_{\theta bo}\in\mathbb{R}^{n\times n}$ and $\boldsymbol{\Gamma}_{\theta do}\in\mathbb{R}^{n\times n}$ are positive definite matrices.

Note that $\hat{\boldsymbol{\theta}}_d$ is obtained by integrating $\dot{\hat{\boldsymbol{\theta}}}_d$, while $\ddot{\hat{\boldsymbol{\theta}}}_d$ is obtained by differentiating $\dot{\hat{\boldsymbol{\theta}}}_d$ with respect to time. By using the estimated signals, a new sliding vector is then defined as

$$\hat{\boldsymbol{e}}_{s\theta}=\dot{\boldsymbol{\theta}}-\dot{\hat{\boldsymbol{\theta}}}_{\mathrm{r}}=\dot{\hat{\boldsymbol{e}}}_\theta+\lambda_\theta\hat{\boldsymbol{e}}_\theta\tag{22}$$

where the reference vector $\dot{\hat{\boldsymbol{\theta}}}_{\mathrm{r}}$ is defined as

$$\dot{\hat{\boldsymbol{\theta}}}_{\mathrm{r}}=\dot{\hat{\boldsymbol{\theta}}}_d-\lambda_\theta\hat{\boldsymbol{e}}_\theta\tag{23}$$

and $\hat{\boldsymbol{e}}_\theta=\boldsymbol{\theta}-\hat{\boldsymbol{\theta}}_d$.

Control input for motor side is now proposed as

$$\boldsymbol{\tau}=\boldsymbol{K}(\boldsymbol{\theta}-\boldsymbol{q})-\boldsymbol{K}_\theta\hat{\boldsymbol{e}}_{s\theta}+\boldsymbol{Y}_\theta(\dot{\hat{\boldsymbol{\theta}}}_{\mathrm{r}},\ddot{\hat{\boldsymbol{\theta}}}_{\mathrm{r}})\hat{\boldsymbol{p}}_\theta\tag{24}$$

where the uncertain parameters $\hat{\boldsymbol{p}}_\theta$ are updated by

$$\dot{\hat{\boldsymbol{p}}}_\theta=-\boldsymbol{\Gamma}_\theta\boldsymbol{Y}_\theta^{\mathrm{T}}(\dot{\hat{\boldsymbol{\theta}}}_{\mathrm{r}},\ddot{\hat{\boldsymbol{\theta}}}_{\mathrm{r}})\hat{\boldsymbol{e}}_{s\theta}\tag{25}$$

Using the estimated signals $\hat{\boldsymbol{\theta}}_d$, $\dot{\hat{\boldsymbol{\theta}}}_d$, and $\ddot{\hat{\boldsymbol{\theta}}}_d$, $\boldsymbol{\tau}$ in Eq.(24) does not require the acceleration information and its derivatives.

3 Closed-Loop Stability Analysis

This section presents stability analysis for closed-loop system with controller Eq.(24).

Substituting the desired input $\boldsymbol{\theta}_d$ into Eq.(8) yields

$$\begin{aligned}\boldsymbol{M}(\boldsymbol{q})\ddot{\boldsymbol{q}}+[\boldsymbol{C}(\boldsymbol{q},\dot{\boldsymbol{q}})+\boldsymbol{D}_q+\omega(\boldsymbol{f}_{\mathrm{e}})\boldsymbol{K}_d]\dot{\boldsymbol{q}}+\\ \boldsymbol{Y}_q(\boldsymbol{q})\tilde{\boldsymbol{p}}_q=\boldsymbol{K}\boldsymbol{e}_\theta+\omega(\boldsymbol{f}_{\mathrm{e}})\boldsymbol{s}-\\ \omega(\boldsymbol{f}_{\mathrm{e}})\boldsymbol{K}_p\arctan(\boldsymbol{\gamma}\boldsymbol{e}_q)+\boldsymbol{\tau}_{\mathrm{e}}\end{aligned}\tag{26}$$

where $\tilde{\boldsymbol{p}}_q=\boldsymbol{p}_q-\hat{\boldsymbol{p}}_q$.

Link-side scalar function V_q is proposed as

$$\begin{aligned}V_q=\frac{1}{2}\dot{\boldsymbol{q}}^{\mathrm{T}}\boldsymbol{M}(\boldsymbol{q})\dot{\boldsymbol{q}}+\frac{1}{2}\tilde{\boldsymbol{p}}_q^{\mathrm{T}}\boldsymbol{\Gamma}_q^{-1}\tilde{\boldsymbol{p}}_q+\\ \omega(\boldsymbol{f}_{\mathrm{e}})\sum_{i=1}^{n}h_i(e_{qi})\end{aligned}\tag{27}$$

where

$$h_i(e_{qi})=K_{pi}\left[e_{qi}\arctan(\gamma_i e_{qi})-\frac{1}{2\gamma_i}\ln(1+\gamma_i^2e_{qi}^2)\right]\tag{28}$$

Taking partial derivative of $h_i(e_{qi})$ with respect to e_{qi} yields

$$\frac{\partial h_i(e_{qi})}{\partial e_{qi}}=K_{pi}\arctan(\gamma_i e_{qi})\tag{29}$$

From Eq.(29), it can be easily concluded that

$$\frac{\partial h_i(e_{qi})}{\partial e_{qi}}\begin{cases}>0 & e_{qi}>0\\ =0 & e_{qi}=0\\ <0 & e_{qi}<0\end{cases}\tag{30}$$

Therefore, $\sum_{i=1}^{n}h_i(e_{qi})$ gets the global minimum value at point $e_{qi}=0$, that is

$$\begin{cases}\forall\boldsymbol{e}_q\in\mathbb{R}^n:\sum_{i=1}^{n}h_i(e_{qi})\geqslant 0\\ \sum_{i=1}^{n}h_i(e_{qi})=0\Leftrightarrow\boldsymbol{e}_q=\boldsymbol{0}\end{cases}\tag{31}$$

Eq.(31) implies that V_q is positive definite, hence, V_q is a Lyapunov function. Differentiating Eq.(27) with respect to time and substituting Eq.(26) into it, we have

$$\begin{aligned}\dot{V}_q=&\frac{1}{2}\dot{\boldsymbol{q}}^{\mathrm{T}}\dot{\boldsymbol{M}}(\boldsymbol{q})\dot{\boldsymbol{q}}+\dot{\boldsymbol{q}}^{\mathrm{T}}\boldsymbol{M}(\boldsymbol{q})\ddot{\boldsymbol{q}}+\\ &\omega(\boldsymbol{f}_{\mathrm{e}})\dot{\boldsymbol{q}}^{\mathrm{T}}\boldsymbol{K}_p\arctan(\boldsymbol{\gamma}\boldsymbol{e}_q)+\tilde{\boldsymbol{p}}_q^{\mathrm{T}}\boldsymbol{\Gamma}_q^{-1}\dot{\tilde{\boldsymbol{p}}}_q=\\ &\frac{1}{2}\dot{\boldsymbol{q}}^{\mathrm{T}}\dot{\boldsymbol{M}}(\boldsymbol{q})\dot{\boldsymbol{q}}+\omega(\boldsymbol{f}_{\mathrm{e}})\dot{\boldsymbol{q}}^{\mathrm{T}}\boldsymbol{K}_p\arctan(\boldsymbol{\gamma}\boldsymbol{e}_q)-\\ &\tilde{\boldsymbol{p}}_q^{\mathrm{T}}\boldsymbol{\Gamma}_q^{-1}\dot{\hat{\boldsymbol{p}}}_q+\dot{\boldsymbol{q}}^{\mathrm{T}}[\omega(\boldsymbol{f}_{\mathrm{e}})\boldsymbol{s}-\omega(\boldsymbol{f}_{\mathrm{e}})\boldsymbol{K}_p\arctan(\boldsymbol{\gamma}\boldsymbol{e}_q)-\\ &\boldsymbol{Y}_q(\boldsymbol{q})\tilde{\boldsymbol{p}}_q]+\dot{\boldsymbol{q}}^{\mathrm{T}}(\boldsymbol{K}\boldsymbol{e}_\theta+\boldsymbol{\tau}_{\mathrm{e}})-\\ &\dot{\boldsymbol{q}}^{\mathrm{T}}[\boldsymbol{C}(\boldsymbol{q},\dot{\boldsymbol{q}})+\boldsymbol{D}_q+\omega(\boldsymbol{f}_{\mathrm{e}})\boldsymbol{K}_d]\dot{\boldsymbol{q}}\end{aligned}\tag{32}$$

Substituting updated law Eq.(10) into Eq.(32) and using Property 2 yield

$$\begin{aligned}\dot{V}_q=&\dot{\boldsymbol{q}}^{\mathrm{T}}(\boldsymbol{K}\boldsymbol{e}_\theta+\boldsymbol{\tau}_{\mathrm{e}})-\dot{\boldsymbol{q}}^{\mathrm{T}}[\boldsymbol{D}_q+\omega(\boldsymbol{f}_{\mathrm{e}})\boldsymbol{K}_d]\dot{\boldsymbol{q}}+\\ &\omega(\boldsymbol{f}_{\mathrm{e}})\dot{\boldsymbol{q}}^{\mathrm{T}}\boldsymbol{s}\end{aligned}\tag{33}$$

Then, motor-side dynamics can be expressed in terms of $\hat{\boldsymbol{e}}_{s\theta}$ as

$$\boldsymbol{B}\dot{\hat{\boldsymbol{e}}}_{s\theta}+\boldsymbol{D}_\theta\hat{\boldsymbol{e}}_{s\theta}+\boldsymbol{K}(\boldsymbol{\theta}-\boldsymbol{q})+\boldsymbol{B}\ddot{\hat{\boldsymbol{\theta}}}_{\mathrm{r}}+\boldsymbol{D}_\theta\dot{\hat{\boldsymbol{\theta}}}_{\mathrm{r}}=\boldsymbol{\tau}\tag{34}$$

Substituting Eq.(24) into Eq.(34) yields

$$\boldsymbol{B}\dot{\hat{\boldsymbol{e}}}_{s\theta}+(\boldsymbol{D}_\theta+\boldsymbol{k}_\theta)\hat{\boldsymbol{e}}_{s\theta}+\boldsymbol{Y}_\theta(\dot{\hat{\boldsymbol{\theta}}}_{\mathrm{r}},\ddot{\hat{\boldsymbol{\theta}}}_{\mathrm{r}})\tilde{\boldsymbol{p}}_\theta=0\tag{35}$$

where $\tilde{\boldsymbol{p}}_\theta=\boldsymbol{p}_\theta-\hat{\boldsymbol{p}}_\theta$.

Multiplying both sides of Eq.(20) with $\hat{\boldsymbol{B}}_{\mathrm{o}}$ and using Eq.(2), we can get

$$B\dot{z}+D_\theta z+k_e e_o=(\hat{B}_o-B)\dot{\phi}+(\hat{D}_{\theta o}-D_\theta)\phi=-Y_{\theta b}(\dot{\phi})\tilde{p}_{\theta bo}-Y_{\theta d}(\phi)\tilde{p}_{\theta do}=-Y_\theta(\phi,\dot{\phi})\tilde{p}_{\theta o} \tag{36}$$

where $\tilde{p}_{\theta bo}=p_{\theta b}-\hat{p}_{\theta bo}$, $\tilde{p}_{\theta do}=p_{\theta d}-\hat{p}_{\theta do}$ and $\tilde{p}_{\theta o}=[\tilde{p}_{\theta bo}^{\mathrm{T}},\tilde{p}_{\theta do}^{\mathrm{T}}]^{\mathrm{T}}$.

Motor-side Lyapunov function is proposed as

$$V_\theta=\frac{1}{2}\hat{e}_{s\theta}^{\mathrm{T}}B\hat{e}_{s\theta}+\frac{1}{2}\tilde{p}_\theta^{\mathrm{T}}\Gamma_\theta^{-1}\tilde{p}_\theta+\lambda_\theta\hat{e}_\theta^{\mathrm{T}}K_\theta\hat{e}_\theta+\frac{1}{2}\tilde{p}_{\theta o}^{\mathrm{T}}\Gamma_{\theta o}^{-1}\tilde{p}_{\theta o}+\frac{1}{2}z^{\mathrm{T}}Bz \tag{37}$$

Differentiating Eq.(37) with respect to time, and substituting Eqs.(21,25,35,36) into it yield

$$\dot{V}_\theta=\hat{e}_{s\theta}^{\mathrm{T}}B\dot{\hat{e}}_{s\theta}+\tilde{p}_\theta^{\mathrm{T}}\Gamma_\theta^{-1}\dot{\tilde{p}}_\theta+2\lambda_\theta\hat{e}_\theta^{\mathrm{T}}K_\theta\dot{\hat{e}}_\theta+\tilde{p}_{\theta o}^{\mathrm{T}}\Gamma_{\theta o}^{-1}\dot{\tilde{p}}_{\theta o}+z^{\mathrm{T}}B\dot{z}=-\hat{e}_{s\theta}^{\mathrm{T}}(D_\theta+K_\theta)\hat{e}_{s\theta}+2\lambda_\theta\hat{e}_\theta^{\mathrm{T}}K_\theta\dot{\hat{e}}_\theta-z^{\mathrm{T}}D_\theta z-z^{\mathrm{T}}K_e e_o \tag{38}$$

Next, for further stability analysis, let Lyapunov function V be constructed as

$$V=V_q+V_\theta \tag{39}$$

Differentiating V with respect to time and substituting Eqs.(11, 33, 38) into it, one obtains

$$\begin{aligned}\dot{V}=&-\dot{q}^{\mathrm{T}}[D_q+\omega(f_e)K_d]\dot{q}-\hat{e}_{s\theta}^{\mathrm{T}}(D_\theta+K_\theta)\hat{e}_{s\theta}-z^{\mathrm{T}}D_\theta z+\dot{q}^{\mathrm{T}}(Ke_\theta+\tau_e)+2\lambda_\theta\hat{e}_\theta^{\mathrm{T}}K_\theta\dot{\hat{e}}_\theta+\omega(f_e)\dot{q}^{\mathrm{T}}s-z^{\mathrm{T}}K_e e_o=\\&-\dot{q}^{\mathrm{T}}[D_q+\omega(f_e)K_d]\dot{q}-\hat{e}_{s\theta}^{\mathrm{T}}(D_\theta+K_\theta)\hat{e}_{s\theta}-z^{\mathrm{T}}D_\theta z+\dot{q}^{\mathrm{T}}(Ke_\theta+\tau_e)+2\lambda_\theta\hat{e}_\theta^{\mathrm{T}}K_\theta\dot{\hat{e}}_\theta-z^{\mathrm{T}}K_e e_o-\omega(f_e)\sum_{i=1}^{n}\gamma_i\dot{q}_i^2\left(\sum_{j=1}^{n}\dot{\theta}_j^2\right)+\\&\omega(f_e)\sum_{i=1}^{n}\{-\alpha_{1i}+[\alpha_{2i}\mathrm{sign}(e_{qi})+\alpha_{3i}\mathrm{sign}(\dot{q}_i)]|e_{qi}|^{1/2}\}\dot{q}_i^2\end{aligned} \tag{40}$$

Note that $e_\theta=\hat{e}_\theta-e_o$ and $z=\dot{\hat{e}}_\theta+k_o e_o$, Eq.(40) can be written as

$$\begin{aligned}\dot{V}=&\dot{q}^{\mathrm{T}}\tau_e-\hat{e}_{s\theta}^{\mathrm{T}}D_\theta\hat{e}_{s\theta}-z^{\mathrm{T}}D_\theta z-\omega(f_e)\sum_{i=1}^{n}\gamma_i\dot{q}_i^2\left(\sum_{j=1}^{n}\dot{\theta}_j^2\right)-[\dot{q}^{\mathrm{T}}\ \hat{e}_\theta^{\mathrm{T}}\ \dot{\hat{e}}_\theta^{\mathrm{T}}\ e_o^{\mathrm{T}}]W[\dot{q}^{\mathrm{T}}\ \hat{e}_\theta^{\mathrm{T}}\ \dot{\hat{e}}_\theta^{\mathrm{T}}\ e_o^{\mathrm{T}}]^{\mathrm{T}}+\\&\omega(f_e)\sum_{i=1}^{n}\{-\alpha_{1i}+[\alpha_{2i}\mathrm{sign}(e_{qi})+\alpha_{3i}\mathrm{sign}(\dot{q}_i)]\left|e_{qi}\right|^{1/2}\}\dot{q}_i^2\end{aligned} \tag{41}$$

where W is given by

$$W=\begin{pmatrix}D_q+\omega(f_e)K_q & -K/2 & 0 & K/2\\ -K/2 & \lambda_\theta^2K_\theta & 0 & 0\\ 0 & 0 & K_\theta & K_e/2\\ K/2 & 0 & K_e/2 & \lambda_o K_e\end{pmatrix} \tag{42}$$

Then Eq.(41) is written as

$$\dot{V}+Q=\dot{q}^{\mathrm{T}}\tau_e \tag{43}$$

where

$$\begin{aligned}Q=&\hat{e}_{s\theta}^{\mathrm{T}}f_\theta\hat{e}_{s\theta}+z^{\mathrm{T}}f_\theta z+\omega(f_e)\sum_{i=1}^{n}\gamma_i\dot{q}_i^2\left(\sum_{j=1}^{n}\dot{\theta}_j^2\right)+[\dot{q}^{\mathrm{T}}\ \hat{e}_\theta^{\mathrm{T}}\ \dot{\hat{e}}_\theta^{\mathrm{T}}\ e_o^{\mathrm{T}}]W[\dot{q}^{\mathrm{T}}\ \hat{e}_\theta^{\mathrm{T}}\ \dot{\hat{e}}_\theta^{\mathrm{T}}\ e_o^{\mathrm{T}}]^{\mathrm{T}}-\\&\omega(f_e)\sum_{i=1}^{n}\{-\alpha_{1i}+[\alpha_{2i}\mathrm{sign}(e_{qi})+\alpha_{3i}\mathrm{sign}(\dot{q}_i)]\left|e_{qi}\right|^{1/2}\}\dot{q}_i^2\end{aligned} \tag{44}$$

Integrating Eq.(43) over $[0,t]$ yields

$$\int_0^t\dot{q}^{\mathrm{T}}(\varepsilon)\tau_e(\varepsilon)\mathrm{d}\varepsilon=V(t)-V(0)+\int_0^tQ(\varepsilon)\mathrm{d}\varepsilon \tag{45}$$

Now, we have the following theorem to state the boundedness of the link-side position error e_q.

Theorem 1 The proposed adaptation and control schemes described by Eqs.(10, 21, 24, 25) ensure the stability of FJR, the boundedness of all state variables and the convergence $e_\theta\to 0$, if external force f_e is bounded, and the control parameters are chosen such that

$$\alpha_{1i}>\eta^{1/2}(\alpha_{2i}+\alpha_{3i}) \tag{46}$$

$$2\lambda_{\min}[W]-1>0 \tag{47}$$

where $\lambda_{\min}[\cdot]$ represents the minimum eigenvalues and η the positive constant to be introduced later.

Proof Let region Ω be defined as follows

$$\Omega=\{e_q\,|\,\|e_q\|\leqslant\eta\} \tag{48}$$

Considering Eq.(46), in region Ω, the following inequality holds

$$\alpha_{1i}-[\alpha_{2i}\mathrm{sign}(e_{qi})+\alpha_{3i}\mathrm{sign}(\dot{q}_i)]\left|e_{qi}\right|^{1/2}>0 \tag{49}$$

If condition Eq.(47) is satisfied, Q is positive. Since Q is positive, we have

$$\int_0^t\dot{q}^{\mathrm{T}}(\varepsilon)\tau_e(\varepsilon)\mathrm{d}\varepsilon\geqslant V(t)-V(0) \tag{50}$$

Remark 2 Eq.(50) demonstrates the passivity of the dynamics between input τ_e and output $\dot{q}$. The passivity shows that at any time the energy stored in the system $V(t)-V(0)$ is less than or equal to the energy introduced from external force. Therefore, the proposed control scheme guarantees the safety between FJR and the surroundings.

If external force f_e is bounded, external torque $\tau_e=J^{\mathrm{T}}(q)f_e$ is also bounded. Note that

$$\int_0^t \dot{\boldsymbol{q}}^{\mathrm{T}}(\varepsilon)\boldsymbol{\tau}_{\mathrm{e}}(\varepsilon)\mathrm{d}\varepsilon \leqslant \frac{1}{2}\int_0^t \left\|\dot{\boldsymbol{q}}(\varepsilon)\right\|^2 \mathrm{d}\varepsilon + \frac{1}{2}\int_0^t \left\|\boldsymbol{\tau}_{\mathrm{e}}(\varepsilon)\right\|^2 \mathrm{d}\varepsilon \tag{51}$$

From Eq.(45) and Eq.(51), we have

$$-V(0)+\int_0^t Q(\varepsilon)\mathrm{d}\varepsilon \leqslant \frac{1}{2}\int_0^t \left\|\dot{\boldsymbol{q}}(\varepsilon)\right\|^2 \mathrm{d}\varepsilon + \frac{1}{2}\int_0^t \left\|\boldsymbol{\tau}_{\mathrm{e}}(\varepsilon)\right\|^2 \mathrm{d}\varepsilon \tag{52}$$

From Eq.(44), $Q \geqslant \lambda_{\min}[\boldsymbol{W}]\left\|\dot{\boldsymbol{q}}\right\|^2$. Therefore, we have

$$\int_0^t \lambda_{\min}[\boldsymbol{W}]\left\|\dot{\boldsymbol{q}}(\varepsilon)\right\|^2 \mathrm{d}\varepsilon \leqslant \frac{1}{2}\int_0^t \left\|\dot{\boldsymbol{q}}(\varepsilon)\right\|^2 \mathrm{d}\varepsilon + \frac{1}{2}\int_0^t \left\|\boldsymbol{\tau}_{\mathrm{e}}(\varepsilon)\right\|^2 \mathrm{d}\varepsilon + V(0) \tag{53}$$

which also implies that

$$\int_0^t (2\lambda_{\min}[\boldsymbol{W}]-1)\left\|\dot{\boldsymbol{q}}(\varepsilon)\right\|^2 \mathrm{d}\varepsilon \leqslant \int_0^t \left\|\boldsymbol{\tau}_{\mathrm{e}}(\varepsilon)\right\|^2 \mathrm{d}\varepsilon + 2V(0) \tag{54}$$

Since $2\lambda_{\min}[\boldsymbol{W}]-1>0$, we can conclude that the boundedness of $\boldsymbol{\tau}_{\mathrm{e}}$ ensures the boundedness of $\dot{\boldsymbol{q}}$. From Eq.(50), we have

$$V(t) \leqslant \int_0^t \dot{\boldsymbol{q}}^{\mathrm{T}}(\varepsilon)\boldsymbol{\tau}_{\mathrm{e}}(\varepsilon)\mathrm{d}\varepsilon + V(0) \tag{55}$$

Since both $\dot{\boldsymbol{q}}$ and $\boldsymbol{\tau}_{\mathrm{e}}$ are bounded, V is also bounded. From Eqs.(27, 37, 39), the boundedness of V ensures the boundedness of all state variables, thus the closed-loop system is stable. In addition, the boundedness of $\hat{\boldsymbol{e}}_{s\theta}$ and $\hat{\boldsymbol{e}}_{\theta}$ ensures the boundedness of $\dot{\hat{\boldsymbol{e}}}_{\theta}$. Hence, $\hat{\boldsymbol{e}}_{\theta}$ is uniformly continuous. Then, From Eq.(44) and Eq.(45), we have

$$\int_0^{+\infty}\left\{\lambda_{\min}[\boldsymbol{W}]\hat{\boldsymbol{e}}_{\theta}^{\mathrm{T}}(t)\hat{\boldsymbol{e}}_{\theta}(t)\right\}\mathrm{d}t \leqslant \int_0^{+\infty} Q(t)\mathrm{d}t = V(0)-V(+\infty)+\int_0^{+\infty}\dot{\boldsymbol{q}}^{\mathrm{T}}(t)\boldsymbol{\tau}_{\mathrm{e}}(t)\mathrm{d}t \tag{56}$$

where the right side is bounded. Hence, $\hat{\boldsymbol{e}}_{\theta} \in L_2(0,+\infty)$ and $\hat{\boldsymbol{e}}_{\theta} \to 0$. Similarly, we can get $\boldsymbol{e}_{\mathrm{o}} \to 0$. Since $\boldsymbol{e}_{\theta} = \hat{\boldsymbol{e}}_{\theta} - \boldsymbol{e}_{\mathrm{o}}$, then $\boldsymbol{e}_{\theta} \to \boldsymbol{0}$. That is, the convergence of $\boldsymbol{\theta} \to \boldsymbol{\theta}_d$ is guaranteed.

The above stability analysis does not depend on specific values of weight factor $\omega(\boldsymbol{f}_{\mathrm{e}})$, and thus, it is applicable to vibration suppression mode, compliance control mode, and also the transition stage. If external force is further negligible, the proposed controller works in vibration suppression mode. Then, the following theorem states the convergence of link-side position error.

Theorem 2 The closed-loop system gives rise to the convergence of link-side position error in vibration suppression mode, if external force $\boldsymbol{f}_{\mathrm{e}}$ is negligible, and the control parameters are chosen such that Eq.(46) and the following condition are satisfied

$$\begin{cases} \lambda_{\theta}^2\lambda_{\min}[\boldsymbol{K}_{\theta}\boldsymbol{D}_q] > \lambda_{\max}[\boldsymbol{K}^2]/4 \\ k_{\mathrm{o}}\lambda_{\min}[\boldsymbol{K}_{\theta}] > \lambda_{\max}[\boldsymbol{K}_{\mathrm{e}}]/4 \\ \lambda_{\min}[\boldsymbol{K}_{\mathrm{e}}]\left\{\lambda_{\mathrm{o}}\lambda_{\min}[\boldsymbol{K}_{\theta}]-\lambda_{\max}[\boldsymbol{K}_{\mathrm{e}}]/4\right\} \\ \left\{\lambda_{\theta}^2\lambda_{\min}[\boldsymbol{K}_{\theta}\boldsymbol{D}_q]-\lambda_{\max}[\boldsymbol{K}^2]/4\right\} > \lambda_{\theta}^2\lambda_{\max}[\boldsymbol{K}_{\theta}^2\boldsymbol{K}^2]/4 \end{cases} \tag{57}$$

Proof Since external force $\boldsymbol{f}_{\mathrm{e}}$ is negligible, we have $\boldsymbol{\tau}_{\mathrm{e}} \to \boldsymbol{0}$. If Eq.(46) and Eq.(57) are satisfied, we have $\dot{V} = -Q \leqslant 0$. From Eq.(41), when $\dot{V} = 0$, $\hat{\boldsymbol{e}}_{s\theta}, \boldsymbol{z}, \dot{\boldsymbol{q}}, \hat{\boldsymbol{e}}_{\theta}, \dot{\hat{\boldsymbol{e}}}_{\theta}, \boldsymbol{e}_{\mathrm{o}}$ are equal to zero. Hence, $\ddot{\boldsymbol{q}}, \boldsymbol{e}_{\theta}$, and $\boldsymbol{s}$ equal zero. Inserting these results into Eq.(8) yields

$$\boldsymbol{g}(\boldsymbol{q}) = -\boldsymbol{K}_p \arctan(\boldsymbol{\gamma}\boldsymbol{e}_q) + \boldsymbol{Y}_q(\boldsymbol{q})\hat{\boldsymbol{p}}_q \tag{58}$$

The use of the adaptation in Eq.(10) ensures the convergence of the prediction error, thus solving Eq.(58) can get $\boldsymbol{e}_q = 0$. Through analysis above, Eq.(58) owns the unique solution $\boldsymbol{q} = \boldsymbol{q}_d$. A direct application of the Lasalle's invariance principle gives Theorem 2.

Remark 3 It can be concluded that the designed controller does not need exact model parameters such as friction, inertia of motor and link side, Coriolis force and gravity, so it has strong practicability.

4 Simulation Experiments

Numerical simulation results demonstrate the effectiveness of the proposed control scheme. The simulation studies are carried out in the two-link FJR as illustrated in Fig.2.

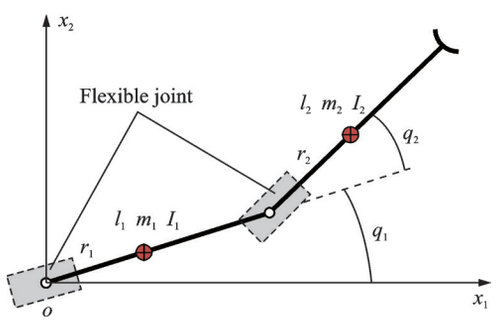

Fig.2 Schematic diagram of two-link FJR

The nominal parameters of FJR's link side and motor side are listed in Table 1.

Table 1 Nominal parameters of FJR

Parameter	Value	Parameter	Value
l_1/m	0.5	r_1/m	0.2
l_2/m	0.5	r_2/m	0.2
m_1/kg	2	I_1/(kg•m^2)	0.5
m_2/kg	2	I_2/(kg•m^2)	0.5
d_{q1}/(N•m•s/rad)	0.2	k_1/(N•m/rad)	100
d_{q2}/(N•m•s/rad)	0.2	k_2/(N•m/rad)	100
$d_{\theta 1}$/(N•m•s/rad)	0.2	B_1/(kg•m^2)	1.5
$d_{\theta 2}$/(N•m•s/rad)	0.2	B_2/(kg•m^2)	1.5

Thus, the dynamic terms in Eqs.(1, 2) can be presented as follows

$$\begin{cases} \boldsymbol{M}(\boldsymbol{q})=\begin{pmatrix} M_{11} & M_{12} \\ M_{21} & M_{22} \end{pmatrix} \\ M_{11}=m_1 r_1^2+m_2(l_1^2+r_2^2+2l_1 r_2\cos q_2)+I_1+I_2 \\ M_{12}=M_{21}=m_2(r_2^2+l_1 r_2\cos q_2)+I_2 \\ M_{22}=m_2 r_2^2+I_2 \\ \boldsymbol{C}(\boldsymbol{q},\dot{\boldsymbol{q}})=\begin{pmatrix} -2m_2 l_1 r_2\dot{q}_2\sin q_2 & -m_2 l_1 r_2\dot{q}_2\sin q_2 \\ m_2 l_1 r_2\dot{q}_1\sin q_2 & 0 \end{pmatrix} \\ \boldsymbol{g}(\boldsymbol{q})=\begin{pmatrix} m_1 g r_1\cos q_1+m_2 g[l_1\cos q_1+r_2\cos(q_1+q_2)] \\ m_2 g r_2\cos(q_1+q_2) \end{pmatrix} \\ \boldsymbol{B}=\begin{pmatrix} B_1 & 0 \\ 0 & B_2 \end{pmatrix},\boldsymbol{K}=\begin{pmatrix} K_1 & 0 \\ 0 & K_1 \end{pmatrix} \\ \boldsymbol{D}_q=\begin{pmatrix} d_{q1} & 0 \\ 0 & d_{q2} \end{pmatrix},\boldsymbol{D}_\theta=\begin{pmatrix} d_{\theta 1} & 0 \\ 0 & d_{\theta 2} \end{pmatrix} \end{cases} \tag{59}$$

The desired position of link side is

$$\boldsymbol{q}_d=[\pi/4 \quad \pi/6]^{\mathrm{T}} \tag{60}$$

First of all, FJR is controlled to track the desired position without external force acting on FJR, which verifies the vibration suppression performance of the proposed scheme. Control parameters of the proposed scheme are chosen as

$$\begin{cases} \boldsymbol{K}_p=\mathrm{diag}\{10,10\},\boldsymbol{K}_d=\mathrm{diag}\{2,2\} \\ \boldsymbol{\gamma}=\mathrm{diag}\{1.5,1.5\} \\ \alpha_{11}=3.8,\alpha_{21}=1,\alpha_{31}=3.5 \\ \alpha_{12}=2.8,\alpha_{22}=0.5,\alpha_{32}=3 \\ \rho_1=1.5,\rho_2=1.5,\lambda_o=100,\lambda_\theta=2 \\ \boldsymbol{K}_e=\mathrm{diag}\{80,80\},\boldsymbol{K}_\theta=\mathrm{diag}\{50,50\} \\ \boldsymbol{\Gamma}_{\theta bo}=\boldsymbol{\Gamma}_{\theta do}=\mathrm{diag}\{10^{-3},10^{-3}\} \\ \boldsymbol{\Gamma}_q=\mathrm{diag}\{5\times10^{-4},5\times10^{-4},5\times10^{-4}\} \\ \boldsymbol{\Gamma}_\theta=\mathrm{diag}\{10^{-3},10^{-3},5\times10^{-3},5\times10^{-3}\} \end{cases} \tag{61}$$

Comparison experiment which employs the proposed scheme but without vibration suppression term $\boldsymbol{s}$ and the same control parameters is carried out. In addition, RRC is also used for comparison. Simulation results are shown in Fig.3.

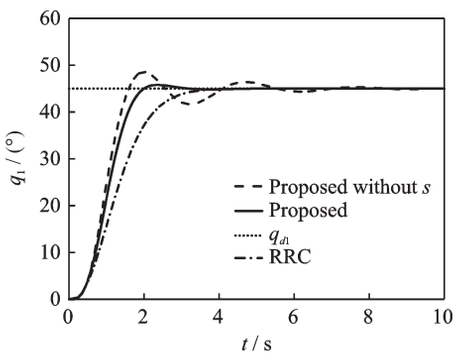

(a) The first link position

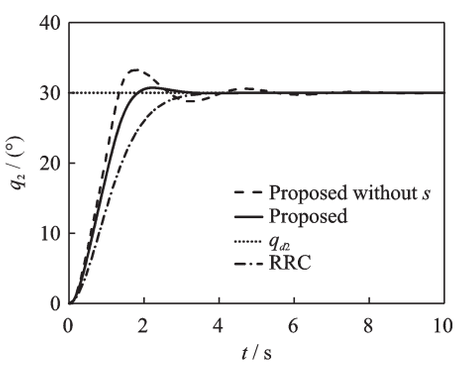

(b) The second link position

Fig.3 Position control for FJR

From Fig.3, it is obvious that both of two links can be driven to the desired position, and the steady state error is small through the above three schemes. However, link side experiences violent oscillation when FJR is in charge of the proposed control scheme but without vibration suppression term $\boldsymbol{s}$. Moreover, the oscillations lead to large overshoot and long settling time. While with the proposed scheme with vibration suppression term $\boldsymbol{s}$, residual vibration is well suppressed. Although the overshoot will also occur, the quantities of overshoot are only 1.06% and 2.36% of two joints, and link-side position converges to the desired position at about 3 s. As a contrast, it takes approximately 4.2 s for link side to converge to the desired position, although no overshoot occurs with RRC.

The regulation criterion of $\boldsymbol{K}_p$ and $\boldsymbol{K}_d$ is the same as PD control. The controller is sensitive to

small error $\boldsymbol{e}_q$ by increasing $\boldsymbol{\gamma}$. A series of simulations are further carried out to test the performance of the vibration suppression term $\boldsymbol{s}$ with different settings of control parameters, which include the followings:

(1) Small parameters [$\alpha_{11}=1$, $\alpha_{21}=0.2$, $\alpha_{31}=0.9$, $\alpha_{12}=0.8$, $\alpha_{22}=0.1$, $\alpha_{32}=1$, $\rho_1=0.3$, $\rho_2=0.3$, others remain the same as Eq.(61)].

(2) Well-tuned parameters [all remain the same as Eq.(61)].

(3) Large parameters [$\alpha_{11}=10$, $\alpha_{21}=4$, $\alpha_{31}=9$, $\alpha_{12}=8$, $\alpha_{22}=2$, $\alpha_{32}=9.5$, $\rho_1=5$, $\rho_2=5$, others remain the same as Eq.(61)].

Simulation results with different settings of control parameters are shown in Fig.4. When the control parameters are set very small (Setting (1)), link positions experience overshoot and the overshoot lead to large oscillation and long settling time. While with well-tuned parameters (Setting (2)), residual vibration is well suppressed. However, if the parameters are set too large (Setting (3)), it takes too long time for link to track the desired position. Besides, after debugging, the values of other parameters must be kept close to the corresponding ones in Eq.(61). If not, violent oscillation, excessive tracking time, steady-state error and even instability will occur.

Then, the end of FJR is exerted an external force during position control, which verifies compliance performance of the proposed scheme. Force region in Eq.(6) is specified as

$$\beta(\boldsymbol{f}_e)=f_{e1}^2+f_{e2}^2-2^2\leqslant 0 \tag{62}$$

where f_{e1} and f_{e2} represent the forces in two coordinates, respectively, the radius $R=2N$, and the parameter κ of weight factor in Eq.(7) is equal to 10.

External force $\boldsymbol{f}_e$ acting on FJR can be described as

$$f_{ei}=\begin{cases}0 & t\leqslant t_1\\ a_i(t-t_1)/\delta t & t_1<t<t_1+\delta t\\ a_i & t_1+\delta t\leqslant t\leqslant t_2-\delta t\\ a_i-a_i(t_2-t)/\delta t & t_2-\delta t<t<t_2\\ 0 & t\geqslant t_2\end{cases} \tag{63}$$

where $t_1=7$ s, $t_2=8.5$ s, $\delta t=0.04$ s, $a_1=1.5$ and $a_2=-2$.

The proposed scheme is employed to control FJR with control parameters as Eq.(61), and link-side positions are shown in Fig.5(a). When the ex-

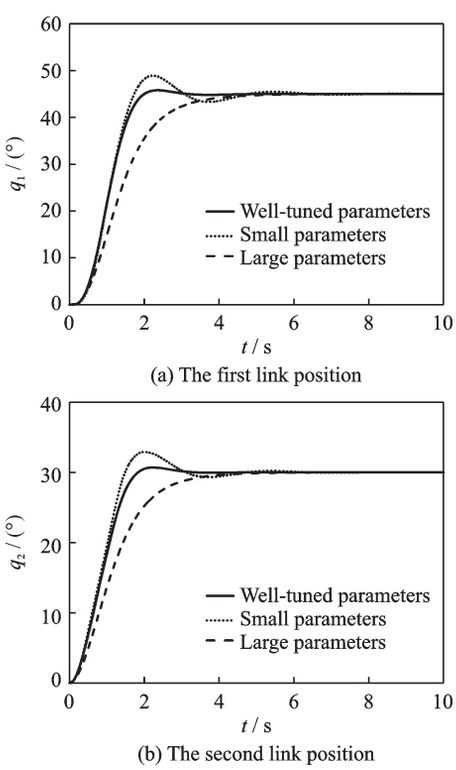

Fig.4 Performance of the proposed controller with different settings of vibration suppression term parameters

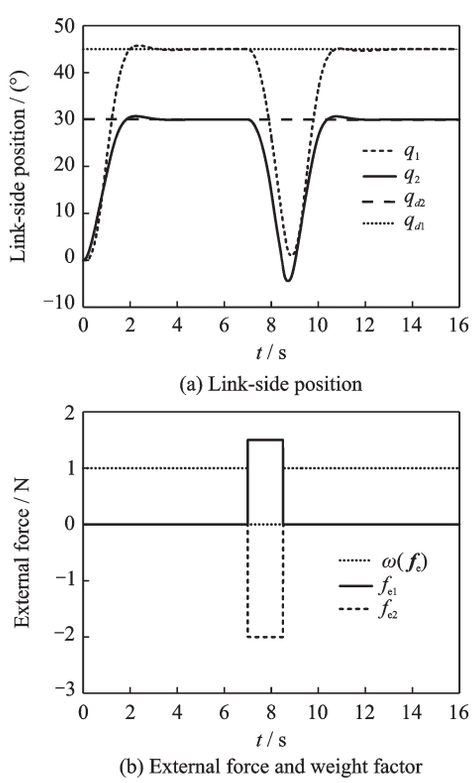

Fig.5 Unified control for FJR

ternal force exceeds the force region such that $\beta(\boldsymbol{f}_e)>0$, weight factor $\omega(\boldsymbol{f}_e)$ decreases from 1 to 0, as shown in Fig.6(b). Then, the proposed controller transits from vibration suppression mode to compliance mode, and FJR becomes passive. The external force pushes link side away from the desired position $\boldsymbol{p}_d$, to guide FJR to move. When external force $\boldsymbol{f}_e$ disappears such that $\beta(\boldsymbol{f}_e)\leqslant 0$, the controller transits to vibration suppression mode again, which drives FJR to track the desired position.

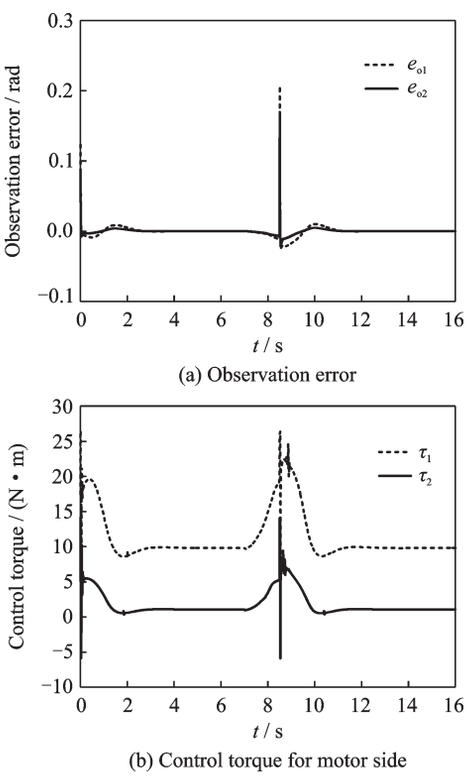

Fig.6 Unified control for FJR

To eliminate the requirement of acceleration information and its derivatives, the observer Eq.(20) is constructed to estimate the desired input $\boldsymbol{\theta}_d$. The observation error is shown in Fig.6(a), which is less than 0.2 rad throughout the course of control. Control input $\boldsymbol{\tau}$ is demonstrated in Fig.6(b) to illustrate the transition performance of the proposed scheme.

It is seen that control input is in a proper range and the proposed scheme ensures a stable and bounded transition of control input between both modes at 7 s and 8.5 s. It's worth noting that, control input of the proposed scheme has a little noise at 8.5 s, which is mainly caused by the abrupt change of link-side desired input $\boldsymbol{\theta}_d$ rather than caused by the proposed control scheme.

5 Conclusions

A unified vibration suppression and compliance control scheme has been proposed for FJR. In the case of vibration suppression mode, the proposed controller allows FJR to track the desired position with better performance in terms of overshoot, settling time and residual vibration suppression. In the case of compliance mode, FJR becomes passive such that external force guides the movement of FJR when the external force exceeds the force region. The smooth and automatic transition among both modes guarantees the safety between FJR and the surroundings. It has been rigorously proved that the closed-loop system is stable, with considering the dynamics uncertainties in both link side and motor side. Simulation results are presented to show the effectiveness of the proposed control scheme.

The proposed control scheme does not consider issues such as input saturation, input constraints and unmodeled dynamics, etc. In real-world applications, for practical FJRs, they always suffer from such issues. In fact, there are already effective solutions to these problems, as suggested in Refs.[24-25]. As a future work, unified vibration suppression and compliance control considering input saturation, input constraints and unmodeled dynamics for FJR which is more suitable for practical application will be further studied.

References

[1] TSAGARAKIS N, MORFEY S, CERDA G M, et al. Compliant humanoid COMAN: Optimal joint stiffness tuning for modal frequency control[C]//Proceedings of 2013 IEEE International Conference on Robotics and Automation. Karlsruhe, Germany: IEEE, 2013: 673-678.

[2] GREBENSTEIN M, ALBU-SCHAFFER A, BAHLS T, et al. The DLR hand arm system[C]//Proceedings of 2011 IEEE International Conference on Robotics and Automation. Shanghai, China: IEEE, 2011: 3175-3182.

[3] ZHANG L, CHEN G. Contact tracking control strategy for space manipulator with snare-type end-effector[J]. Transactions of Nanjing University of Aeronautics and Astronautics, 2019, 36(6): 995-1003.

[4] WANG Congqing, PEI Xiwu, WU Pengfei. Composite control of on-orbit operation of free-floating space flexible manipulator with rigid load[J]. Journal of Nanjing University of Aeronautics and Astronautics, 2012, 44(4): 452-457.(in Chinese)

[5] TOMEI P. A simple PD controller for robots with elastic joints[J]. IEEE Transactions on Automatic Control, 1991, 36(10): 1208-1213.

[6] KIM M J, CHUNG W K. Disturbance-observer-based PD control of flexible joint robots for asymptotic convergence[J]. IEEE Transactions on Robotics, 2015, 31(6): 1508-1516.

[7] JIN M, LEE J, TSAGARAKIS N G. Model-free robust adaptive control of humanoid robots with flexible joints[J]. IEEE Transactions on Industrial Electronics, 2017, 64(2): 1706-1715.

[8] MOBAYEN S, TCHIER F. Nonsingular fast terminal sliding-mode stabilizer for a class of uncertain nonlinear systems based on disturbance observer[J]. Scientia Iranica, 2017, 24(3): 1410-1418.

[9] HAGHIGHI D A, MOBAYEN S. Design of an adaptive super-twisting decoupled terminal sliding mode control scheme for a class of fourth-order systems[J]. ISA Transactions, 2018, 75: 216-225.

[10] PALLI G, MELCHIORRI C, LUCA A D. On the feedback linearization of robots with variable joint stiffness[C]//Proceedings of 2008 IEEE International Conference on Robotics and Automation. Pasadena, CA, USA: IEEE, 2008: 1753-1759.

[11] PETIT F, ALBU-SCHAFFER A. State feedback damping control for a multi DOF variable stiffness robot arm[C]//Proceedings of 2011 IEEE International Conference on Robotics and Automation. Shanghai, China: IEEE, 2011: 5561-5567.

[12] MIYAZAKI F, KAWAMURA S, MATSUMORI M, et al. Learning control scheme for a class of robot systems with elasticity[C]//Proceedings of IEEE Conference on Decision and Control. Athens, Greece: IEEE, 1986: 74-79.

[13] SARDELLITTI I, MEDRANA-CERDA G A, TSAGARAKIS N, et al. Gain scheduling control for a class of variable stiffness actuators based on lever mechanisms[J]. IEEE Transactions on Robotics, 2013, 29: 791-798.

[14] CONKER C, YAVUZ H, BILGIC H. A review of command shaping techniques for elimination of residual vibrations in flexible-joint manipulators[J]. Journal of Vibroengineering, 2016, 18: 2947-2958.

[15] SUN T, LIANG D, SONG Y. Singular-perturbation-based nonlinear hybrid control of redundant parallel robot[J]. IEEE Transactions on Industrial Electronics, 2018, 65(4): 3326-3336.

[16] LIU H, CUI S P, LIU Y W, et al. Design and vibration suppression control of a modular elastic joint[J]. Sensors, 2018. DOI: 10.3390/s18061869.

[17] SUN L, YIN W, WANG M, et al. Position control for flexible joint robot based on online gravity compensation with vibration suppression[J]. IEEE Transactions on Industrial Electronics, 2018, 65(6): 4840-4848.

[18] CAO Q, LI S, ZHAO D. Finite-time position/force control for flexible joint manipulators[C]//Proceedings of the 33rd Chinese Control Conference. Nanjing, China: IEEE, 2014: 2346-2351.

[19] OTT C, ALBU-SCHAFFER A, KUGI A, et al. On the passivity-based impedance control of flexible joint robots[J]. IEEE Transactions on Robotics, 2008, 24(2): 416-429.

[20] LI X, PAN Y, CHEN G, et al. Adaptive human-robot interaction control for robots driven by series elastic actuators[J]. IEEE Transactions on Robotics, 2017, 33(1): 169-182.

[21] LI X, PAN Y, CHEN G, et al. Multi-modal control scheme for rehabilitation robotic exoskeletons[J]. The International Journal of Robotics Research, 2017, 39(5/6/7): 759-777.

[22] SPONG M W. Modeling and control of elastic joint robots[J]. Journal of Dynamic Systems, Measurement, and Control, 1987, 109(4): 310-319.

[23] ISAI G V, IVAN S R, MANUEL M H, et al. Impedance adaptive controller for a prototype of a whiplash syndrome rehabilitation device[J]. Mathematical Problems in Engineering, 2019(3): 1-21.

[24] SUN N, FU Y, YANG T, et al. Nonlinear motion control of complicated dual rotary crane systems without velocity feedback: Design, analysis, and hardware experiments[J]. IEEE Transactions on Automation Science and Engineering, 2020, 17(2): 1017-1029.

[25] SUN N, LIANG D K, WU Y M, et al. Adaptive control for pneumatic artificial muscle systems with parametric uncertainties and unidirectional input constraints[J]. IEEE Transactions on Industrial Informatics, 2020, 16(2): 969-979.

Acknowledgements This work was supported by the National Key R&D Program of China (No.2017YFB1300400) and the National Natural Science Foundation of China (No. 51805107).

Authors Mr. **CUI Shipeng** received the B.S. degree in mechatronics engineering from Heilongjiang Institute of Science and Technology in 2010 and the M.S. degree in naval architecture and marine engineering from Harbin Engineering University in 2013. In 2013, he joined College of Mechanical Engineering, Harbin Institute of Technology. He is currently pursuing the Ph.D. degree with Harbin Institute of Technology. His research interests include structural design and control of flexible joint robot.

Dr. **SUN Yongjun** received the B.S. degree in mechatronics engineering from Harbin Engineering University in 2008, and the M.S. and the Ph.D. degrees in mechatronics engineering from Harbin Institute of Technology in 2010 and 2016, respectively. He is currently an assistant professor of Harbin Institute of Technology. His research interests include multi axis force/torque sensor and space robotics.

Author contributions Mr. **CUI Shipeng** designed the control algorithm and wrote the manuscript. Dr. **SUN Yongjun** conducted the simulation experiment and simulation data. Profs. **LIU Yiwei** and **LIU Hong** contributed to the discussion and background of the study. All authors commented on the manuscript draft and approved the submission.

Competing interests The authors declare no competing inrests.

(Production Editor: XU Chengting)

柔性关节机械臂振动抑制/柔顺统一控制

崔士鹏，孙永军，刘伊威，刘　宏

(哈尔滨工业大学机器人技术与系统国家重点实验室，哈尔滨 150001，中国)

摘要：提出了一种可同时实现柔性关节机器人振动抑制控制和柔顺控制的自适应控制策略。所提出的控制策略为柔性关节机器人提供了振动抑制控制模式和柔顺控制模式的统一方案，将两种控制模式整合到一个控制器中，避免了设计两种控制器并在两种控制器之间切换，实现了两种控制模式的平稳过渡。本文还考虑了机器人连杆端和电机端动力学模型的不确定性，并通过李雅普诺夫定理证明了闭环系统的稳定性。仿真结果表明：所提出的控制策略具有良好的控制性能。

关键词：自适应控制策略；振动抑制；柔顺性；柔性关节机器人；稳定性